RESEARCH ARTICLE

Macromolecular Rapid Communications
www.mrc-journal.de

Hydrophobic Aerogels from Vinyl Polymers Derived from Radical Polymerization: Proof-of-Concept

Claudia Adolfs, Razan Altarabeen, Leon Kimmritz, Lara Gibowsky, Baldur Schroeter, Sabine Beuermann, and Irina Smirnova**

Hydrophilicity is one important drawback of bio-based aerogels. To overcome this issue, a novel approach for the preparation of mesoporous, water repellent aerogels is introduced, which combines synthesis of cross-linked bio-based copolymers from methacrylate copolymerizations, followed by solvent exchange and supercritical drying steps. The influence of monomers with different nonpolar ester groups (methyl, vanillin, tetrahydrofurfuryl) on textural properties and water contact angles of the dry products is assessed. Final aerogels show generally high overall porosities (≈96%), low densities (0.07–0.11 g cm^{-3}) as well as fine, mainly mesoporous networks, and specific surface areas in the range of 120–240 m^2 g^{-1}. Hereby, choice of the methacrylate ester groups results in differences of the resulting pore-size distributions. Water repellency tests show stable static water contact angles in the hydrophobic range (≈100°) achieved for the substrate containing the vanillin ester group. On the contrary the other substrates absorb water quickly, which indicates a decisive role of the ester group. The presented approach opens up a new pathway to bio-based aerogels with intrinsic hydrophobicity. It is suggested that the properties are tailored by the choice of the monomer structure, hence enabling further adaption and optimization of the products.

1. Introduction

Aerogels are advanced solid materials with distinguished high specific surface area (S_V) in the range of several hundred of up to >1000 g^2 m^{-1} and high porosity.[1] The first and most extensively studied aerogel type was already discovered in the 1930s and is based on inorganic silica.[2] Since then, numerous fundamental studies showed that transformation of wet gels (pores filled with solvent) to dry aerogels (pores filled with air) with sufficient (meso)-porosity and according specific surface area can generally be achieved by supercritical-CO_2 extraction of the solvent. Up to now this method is state of the art and the most general drying process in aerogel production.[3–5]

Recent sustainability efforts have sparked increased interest in biopolymer based aerogels, which can be synthesized from widely available biopolymers such as, e.g., cellulose, alginate, starch, or chitosan.[1,6] Due to their superior mechanical properties (e.g., elasticity), low toxicity, and biocompatibility they can be employed in different areas as compared to silica aerogels, e.g. in the food and pharma sector, or as adsorbents.[4,7,8]

The main challenge with handling and storage of these materials lies in their hydrophilic nature, which originates from the high surface density of polar OH-groups of most biopolymers. The surface's hydrophilicity promotes moisture penetration into the inner pore structure of aerogels, resulting in the collapse of mesopores and subsequent loss of, e.g., mechanical and insulating properties.[1,9] Recent studies have focused on overcoming this issue, for example by either surface hydrophobization or functionalization[1,10] (using, e.g., silane derivatives or alkyl aldehydes)[11,12] or other postmodifications such as (external) surface coating via cold plasma and chemical vapor deposition.[9,13]

While these methods might lead to liquid water repellency and protection against moisture in specific cases, they represent an additional process step (leading to higher process costs) and demand in many cases the use of hazardous chemicals. In addition, the postmodification step alters the aerogel's properties: for instance, in case of (external) spray coating, coating material might potentially enter the porous network of the aerogel causing changes or collapse of pores.[14,15] Summarized, the hydrophilic nature of biopolymer aerogels poses nonsolved challenges as hydrophobicity and other targeted/desirable properties need to be balanced in the final aerogel. Moreover, if environmental sustainability is a key concern, biocompatible hydrophobic

C. Adolfs, L. Kimmritz, S. Beuermann
TU Clausthal
Arnold-Sommerfeld-Str. 4, 38678 Clausthal-Zellerfeld, Germany
E-mail: sabine.beuermann@tu-clausthal.de
R. Altarabeen, L. Gibowsky, B. Schroeter, I. Smirnova
Hamburg University of Technology
Institute of Thermal Separation Processes
Eißendorfer Straße 38 (O), 21073 Hamburg, Germany
E-mail: irina.smirnova@tuhh.de

The ORCID identification number(s) for the author(s) of this article can be found under https://doi.org/10.1002/marc.202400147

DOI: 10.1002/marc.202400147

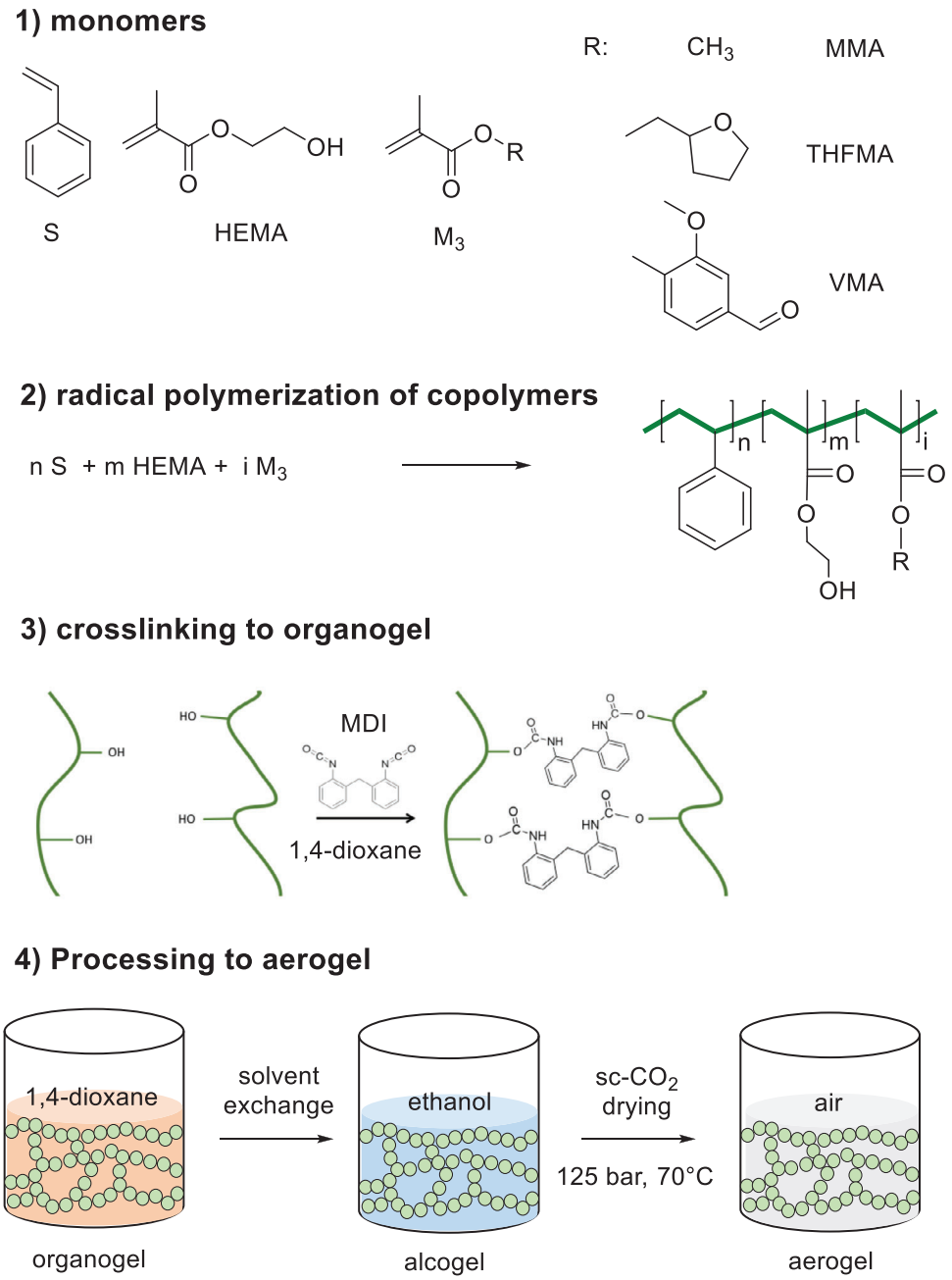

Figure 1. Overall reaction and processing scheme.

agents should be used to ensure the aerogel remains eco-friendly throughout its lifecycle.

In our approach, we intend to synthesize intrinsic hydrophobic aerogels via radical copolymerization of vinyl monomers, e.g. such as styrene and methacrylates with hydrophobic side chains (**Figure 1**, step 2). In order to achieve a high biorenewable carbon content, the methacrylates tetrahydrofurfuryl methacrylate (THFMA) and vanillin methacrylate (VMA) were selected. The ester group of THFMA may be derived from hemicellulose[16] and the vanillin ester group of VMA is originating from lignin.[17,18] The biorenewable carbon content is 56%[16] for THFMA and 67% for VMA. Although methacrylic acid is so far not produced from biorenewable feedstocks, several methods are currently discussed and availability of bio-based methacrylic acid is a question of time.[19] In addition, hydroxy ethyl methacrylate (HEMA) is used as comonomer to introduce the OH-group required for cross-linking. The polymer chains are cross-linked with commercially available bifunctional methylene diphenyl diisocyanate (MDI) to build up a porous urethane-based organogel (Figure 1, step 3).

Overall, we aim to answer the questions whether further processing of thus generated organogels via solvent exchange

from 1,4-dioxane to ethanol (EtOH) and supercritical CO_2-drying (Figure 1, step 4) results in mesoporous aerogels, and whether the final materials show hydrophobic surface properties. Fundamental insights are provided by characterization of the final products' textural properties and assessment of the liquid water repellency.

2. Results and Discussion

2.1. Copolymerization and Gel Formation

In the first step, radical copolymerizations of styrene, HEMA, and a third methacrylate monomer (M_3) with different ester groups were performed (Figure 1, step 2). Hereby, the choice of the monomers was based on their different functionality and availability, as detailed in the following. The use of HEMA is essential, because the OH-group is required for cross-linking. As M_3, THFMA and VMA were chosen, since the ester groups tetrahydrofurfuryl and vanillin may be derived from bio-based feedstocks. MMA was used as alternative methacrylate with significantly smaller ester group as compared to THFMA and VMA, thus, allowing for investigation into the influence of steric effects on the resulting aerogels textural and water repellent properties. Styrene is used since copolymers containing styrene and methacrylate units are already used in large scale and its synthesis is generally well understood.[20] CTA is added to the polymerization mixture in order to limit the molar masses and to facilitate the subsequent dissolution of the obtained copolymers in 1,4-dioxane, which is used as solvent for the cross-linking reaction. To prepare stable organogels the copolymers are cross-linked via reaction of the OH-group originating from HEMA and a diisocyanate resulting in the formation of urethane groups, which serve as covalent cross-links between the polymer chains (Figure 1, step 3). For cross-linking the commercial product Desmodur VP.PU 10WB94 is used, which contains oligomers of MDI.[21] In order to verify cross-linking and to assess the purity of the final aerogel, FT-IR spectra of the samples were taken in the various stages as a copolymer, organogel, and aerogel. As an example, the characteristic changes during processing are shown for the THFMA containing samples in **Figure 2**.

In the following, all peak assignments are based on Socrates.[22] The broad band at 3440 cm^{-1} in the copolymer spectrum is assigned to the OH-group of HEMA. Since the peak is not visible in the organogel spectrum, the OH-group is fully converted by reaction with the isocyanate. The spectra of the organogel and the aerogel show a broad peak at 3340 cm^{-1} which is assigned to the N–H-vibration of the urethane group. In the case of the organogel the peak at 2275 cm^{-1} is indicative of –N=C=O of the isocyanate. The finding indicates an excess of isocyanate in the reaction mixture, because the band assigned to the OH-group has fully disappeared. Since the amount of isocyanate used was based on the initial amount of HEMA contained in the polymerization mixture, during copolymerization HEMA was not fully incorporated in the copolymer. After cross-linking, the spectrum of the organogel shows also two new signals in the range of ≈1515–1600 cm^{-1} (highlighted area). The peak at 1600 cm^{-1} corresponds to the aromatic C–C bond of MDI, and the peak at approx. 1520 cm^{-1} originates from urethane C=O. After removing the solvent in the aerogel, the isocyanate peak

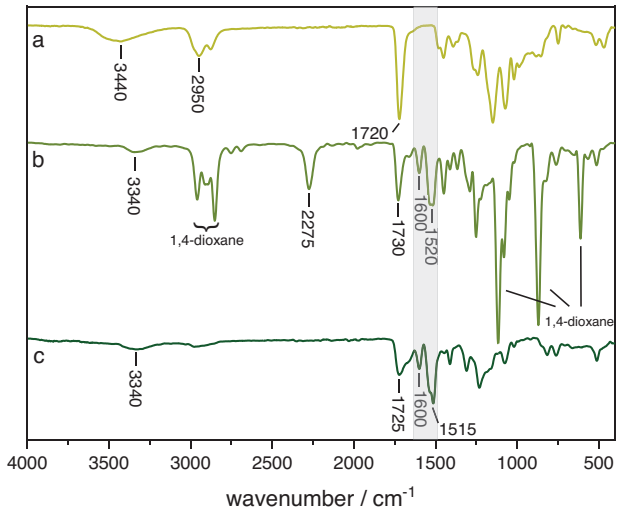

Figure 2. FT-IR spectra of the sample consisting of tetrahydrofurfuryl methacrylate (THFMA), hydroxy ethyl methacrylate (HEMA), and styrene. a) Refers to the copolymer, b) to the cross-linked organogel containing 1,4-dioxane, and c) to the aerogel.

disappeared completely showing that MDI was washed out during aerogel processing steps. The characteristic changes in the IR spectrum are also observed for the other systems with either VMA or MMA instead of THFMA. The spectra are given as Figures S1 and S2 (Supporting Information).

2.2. Properties of Substrates Dried with Supercritical CO_2

Supercritical drying of alcogels resulted in flat, pellet-like, dry polymeric and stiff gels with a height of ≈2–4 mm and diameters in the range of 1.6 to 2.0 cm (**Figure 3a**). Based on these values, the linear shrinkage of substrates during processing from organogel to aerogel was estimated. A shrinkage of 32% was determined for the #MMA sample, of 28% for the #VMA sample, and of 39% for the #THFMA sample. Interestingly, the main shrinkage was observed during the solvent exchange from organogel to alcogel, while up to no shrinkage occurred during supercritical drying (Figure 3a). The further assessment of the samples involved the examination of their skeletal density, envelope density, and overall porosity in order to determine the potential of their classification as "aerogels". The envelope density ranged from 0.07 to 0.11 g cm^{-3}, while skeletal density ranged from 1.6 to 2.9 g cm^{3}: with these values, the overall porosity of the materials was estimated to be in the range between 95.8% and 96.1% (**Table 1**). It can be inferred that the polymerization process for the three samples #MMA, #VMA, and #THFMA followed by solvent exchange with ethanol and supercritical CO_2-drying has effectively yielded lightweight porous materials with high overall porosity falling within the typical range observed for classical aerogels.[22] Assessment of the mechanical strength via uniaxial compression tests showed nonbrittle behavior of samples and no breakage up to max. applied force of 500 N was determined in all cases (despite stress concentration on defined points of the samples) (Figure S3, Supporting Information). Given that the slope of the force–distance relation in the range > 100 N showed a

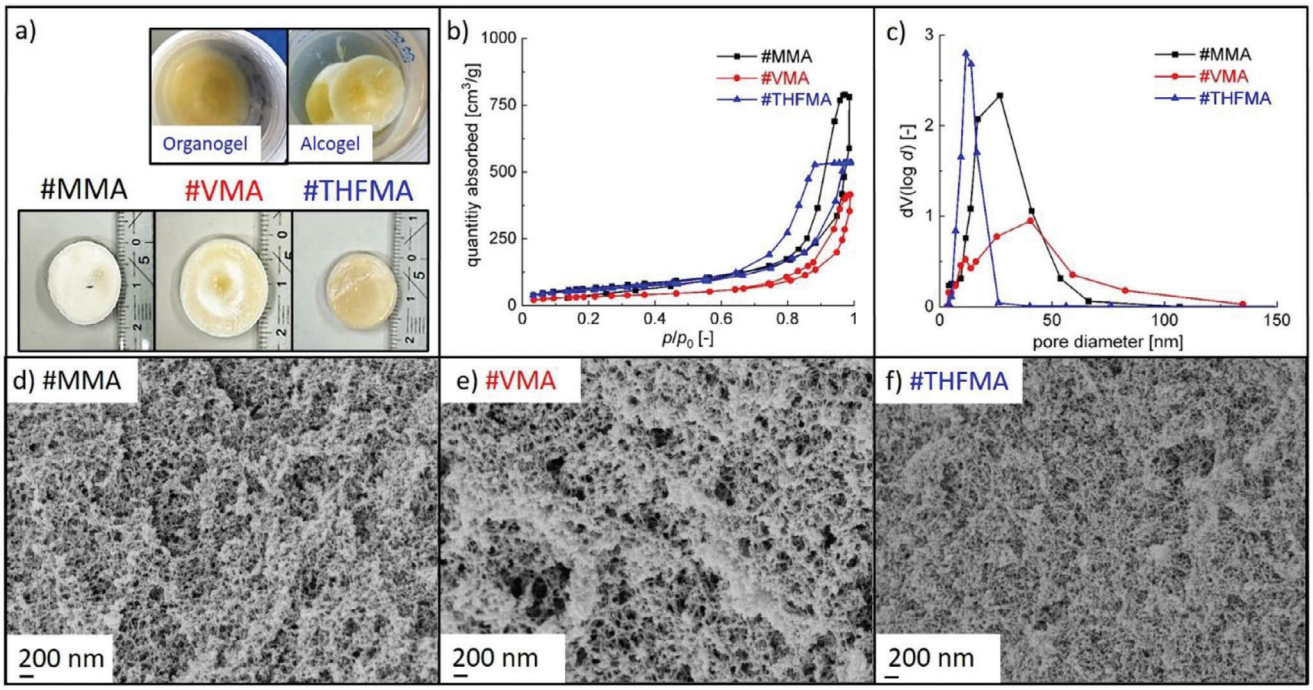

Figure 3. a) Images of organogel, alcogel (example: tetrahydrofurfuryl methacrylate (THFMA) samples) and aerogel substrates b) nitrogen physisorption isotherms c) pore size distributions derived via Barrett–Joyner–Halendia (BJH) method. Lines are drawn to guide the eye. d–f) Scanning electron microscopy (SEM) images of inner porous structure of the aerogel samples taken at 50 000 × Magnification.

similar behavior in all cases, it is proposed that the choice of the side chain has no significant influence on mechanical properties. Thermal analyses of the samples indicate high thermal stability. Up to temperatures of 286 °C, 297 °C, and 311 °C 90% of the residual mass of the samples #MMA, #VMA, and #THFMA, respectively, is retained. The TGA curves are given as Figure S4 (Supporting Information).

Isotherms of nitrogen physisorption measurements showed for all three samples a type IV hysteresis, which is typical for mesoporous adsorbents (Figure 3b).[23] Fundamental information on the characteristics of the pore networks is provided by the shape of the hysteresis loop: #MMA and #VMA exhibit an H3-like shape, which is generally observed for materials of mixed meso- to macroporous nature.[23] In contrast, the isotherm shape of sample #THFMA is indicative for a mesoporous network in the range of small mesopores with narrow pore size distribution, but might also be associated with other effects during nitrogen sorption (e.g., pore blocking, network effects in complex structures).[23] Estimation of the pore size distribution via the Barrett–Joyner–Halendia (BJH) method suggests indeed, that sample #THFMA exhibits the narrowest pore size distribution among the samples, characterized by the smallest mean pore diameter $d_{meso,\,mean}$ and a maximum mesopore size of ≈26 nm, while samples #MMA and #VMA exhibit broader distributions with largest pores estimated to be in the range of small macropores (≈50–130 nm) (Figure 3c). Accordingly, samples show a significant specific surface area of up to 240 $m^2\ g^{-1}$, whereas changes in between samples can be attributed to different mesopore volumes V_{meso} and pore sizes (Table 1).

Results from nitrogen physisorption are consistent with scanning electron microscopy (SEM) images of cut-open samples: in all cases, continuous and homogenous mainly mesoporous, fibrous networks without presence of larger macropores are visible (Figure 3d–f, for images of different magnification we refer to Figure S5, Supporting Information), while images of sample #VMA verify the presence of small macropores. Observed fibrillar pore networks are typical for biopolymer aerogels and contribute to their nonfragility (in contrast to colloidal silica aerogels).[24] The absence of larger macropores and a network formed by rigid covalent cross-links between polymer chains

Table 1. Textural properties of aerogels derived from polymerization of different bio-based methacrylate copolymers cross-linked with methylene diphenyl diisocyanate (MDI).

Sample	Monomer M3	ρe [g cm^{-3}]	ρs [g cm^{-3}]	ϵ [%]	S_v [$m^2\ g^{-1}$]	V_{meso} [$cm^3\ g^{-1}$]	$d_{meso,\,mean}$ [nm]
#MMA	Methyl methacrylate	0.07 ± 1.10^{-3}	1.6 ± 3.10^{-2}	96	241	1.3	20.0
#VMA	Vanillin methacrylate	0.07 ± 7.10^{-5}	1.8 ± 3.10^{-2}	96	119	0.68	21.7
#THFMA	Tetrahydrofurfuryl methacrylate	0.11 ± 8.10^{-4}	2.9 ± 1.10^{-1}	96	210	0.88	15.8

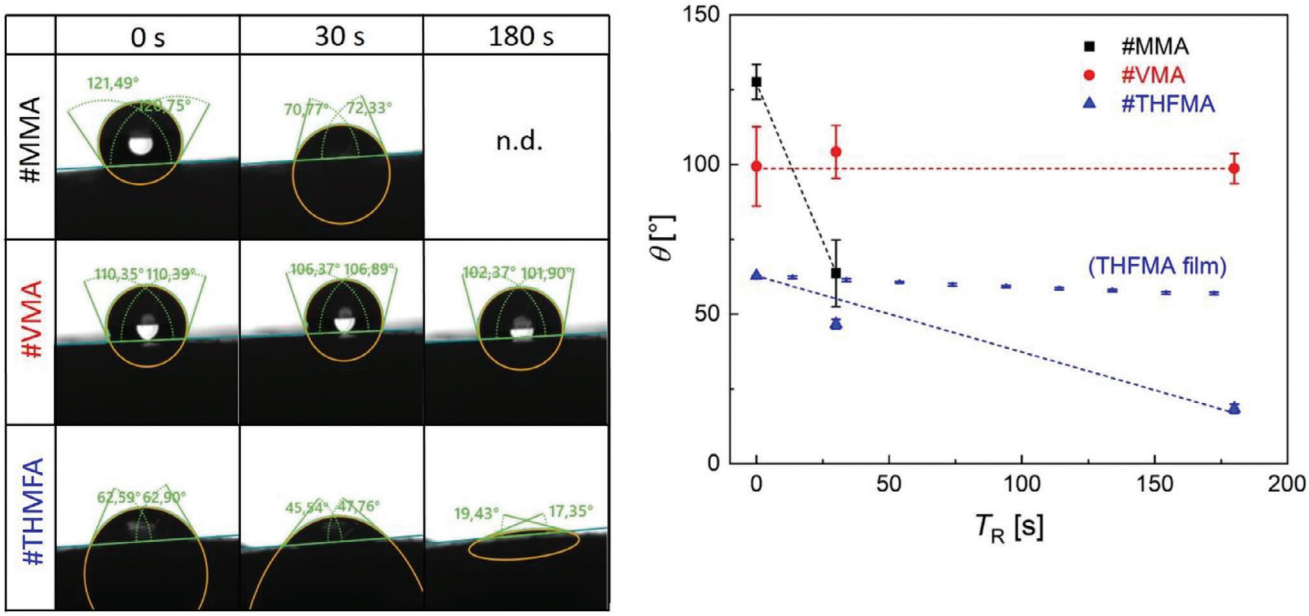

Figure 4. Results of static water contact angle measurements on selected aerogel substrates at different residence times after application of the droplet. Left: raw data images. Right: θ in dependence of the residence time T_R. Error bars correspond to the standard deviation of threefold determinations; dashed lines are drawn to guide the eye.

may contribute to the mechanical stability and nonflexible behavior.

One possible explanation for sample #THFMA being the aerogel with the finest pore structure might be rooted in the reaction mechanism: while the copolymers are obtained from radical polymerizations, the radicals may also induce a side reaction. It is known that the tetrahydrofurfuryl ring in THFMA exhibits high sensitivity to heat and light, making it susceptible to a radical-induced ring-opening reaction.[25,26] This reaction could serve as an additional mechanism for cross-linking, contributing to the formation of a dense and fine pore distribution. Moreover, the copolymerization of VMA has resulted in a broader and larger pore size distribution of #VMA. This finding could be attributed to the lower reactivity of the VMA.[27] As a consequence a copolymer composition drift occurs with increasing conversion and the HEMA content in the copolymer molecules varies, thus, leading to unevenly distributed cross-links.

Although up to now no single definition comprehensively captures the entire range of materials referred to as aerogels in the scientific literature, our results are clearly showing that properties of our products align with key criteria mentioned in recent works, including a high degree of porosity, presence of a significant specific surface area > 100 m^2 g^{-1}, and an open, three-dimensional mainly mesoporous solid network (as opposed to sponges, most cryogels or open foams which consist primarily of macropores).[22,28,29] Accordingly produced materials can be classified as aerogels, whereas the choice of monomers induces changes in the resulting pore structures.

2.3. Liquid Water Repellency

In order to assess the ability of the samples #MMA, #VMA, and #THFMA to withstand contact with polar liquids, static water contact angle (θ) measurements were carried out. The spreadability of a water droplet on a solid surface might principally be influenced by the surface polarity and surface roughness, whereas in the case of water contact angles $\theta > 90°$ the solid surface is considered to be hydrophobic. Due to the open porous nature of aerogels there is, however, also the possibility that the water droplet is absorbed into the aerogels body due to capillary forces (despite hydrophobic surface properties), resulting in deformation of the substrate and pore collapse.[9] In the case of absorption, there is no generally established procedure for the overall quantification of an equilibrium contact angle since the actual value of θ depends on numerous factors (e.g., residence time of the droplet on the surface, overall droplet volume, porosity, pore diameter, and permeability of the substrate).[30] In order to address this issue, θ was determined at three distinct residence times after application of the droplet on the substrates surface respectively: 1) immediately after droplet application (initial contact angle θ_I), 2) after 30 s, and 3) after 180 s.

If possible effects of surface roughness and porosity are neglected, the initial contact angle should be representative for the hydrophilicity/hydrophobicity of the individual copolymers. High initial contact angles in the hydrophobic range were determined for the #MMA and #VMA samples (θ_I (#MMA) = 130°, θ_I(#VMA) = 99°) which shows the contribution of methyl and phenolic side chains toward hydrophobicity (**Figure 4**). In case of the #THFMA sample, a significantly lower initial contact angle (θ_I (#THFMA = 63°) in the hydrophilic range is indicative for the ring opening of the tetrahydrofurfuryl group (see Section 2.2). In order to assess if the initial contact angle is influenced by the presence of pores, $\theta_{I,\#THFMA}$ was compared with θ_I of a nonporous #THFMA film (Figure S6, Supporting Information). Hereby, no difference in the initial contact angles between film and aerogel samples was determined. Furthermore, laser

confocal microscopy revealed that #VMA and #THFMA samples exhibit smooth, homogenous surfaces as, e.g., reflected in the absolute average values of the roughness profiles R_a (≈1.0–1.5 µm) while #MMA shows a slightly increased surface roughness (R_a = 5.3 µm) (Table S2, Figure S7, Supporting Information). While roughness principally affects the wettability (e.g., high roughness reduces wettability in case of hydrophobic materials and consequently the contact angle increases with the relative steepness of surface features), it is suggested that pronounced differences of θ_I between samples in this work are mainly related to the chemical nature of the copolymer.[31]

Differences between the aerogel and film samples were observed for the time dependent behavior of θ. The #THFMA sample showed a nearly complete absorption of the water drop accompanied by a decrease of θ after a relative short residence time (approx. 3 min). Since θ stayed mostly constant in case of the THFMA film (Figure S6, Supporting Information), the course of θ in case of the #THFMA sample is attributed to the presence of pores and absorption of the water droplet into the inner part of the sample. An even faster penetration (<60 s) of the droplet was determined in case of #MMA. This result suggests that a low surface polarity of the copolymer alone is not sufficient to prevent water absorption.

A stable contact angle in the hydrophobic range and no penetration of the droplet into the pore structure was observed in case of the vanillin side chain containing substrate (#VMA). Taking the comparably high similarity of the pore structures and overall porosities between different aerogel samples into account (with #VMA featuring slightly larger pores than the others), it seems reasonable that differences in the water absorption behavior are connected to other sample properties: we surmise that the size of the hydrophobic functionality might play a decisive role, with the comparably "bulky" vanillin group providing the best prevention against liquid water absorption. While the results in this section show that the presented approach allows the synthesis of hydrophobic, liquid water repellent aerogels without postmodification, more in depths studies are necessary to determine and quantify the role of different factors influencing the water uptake (e.g., pore sizes and morphology, choice of side chain in the copolymer and monomer ratio during polymerization).

3. Conclusion

In this work, a new pathway toward hydrophobic aerogels based on covalent cross-linking of methacrylic copolymers with different and partially bio-based ester groups is presented. While our results show that products obtained after supercritical drying can be classified as aerogels with water repellent properties (if vanillin groups are introduced into the system), further investigations beyond this proof-of-concept study are necessary to obtain a deeper understanding of the processes. For instance, our tests showed that liquid water absorption can be prevented by choice of the monomers, but the effects of moisture entering the inner pores of the products in presence of gaseous water have still to be investigated. Furthermore, a multiparameter study regarding monomer ratios would lead to deeper and quantitative understanding about the influence of each monomer on textural properties, the latter being necessary for control and optimization of the pore structure. One benefit of our approach lies in its flexibility, leading to an enhanced control and tailorability as compared to the classical biopolymer-to-aerogel routes, since the introduction of numerous different functional groups via variation of methacrylic monomers (e.g., with longer nonpolar or functional ester groups) is easily possible.

4. Experimental Section

Materials: 1,4-Dioxane (Grüssing, 99%), HEMA (Alfa Aesar, 97%), methyl methacrylate (MMA, Acros, 99%, 10–110 ppm MEQH), methacrylic anhydride (Sigma Aldrich, 94%, 2000 ppm Topanol A), Desmodur VP.PU 10WB94 NCO-Content: 31.0—33.5% (Covestro), sodium chloride (NaCl, Riedel, 99.5%), sodium bicarbonate (Roth, 99%), sodium hydroxide (NaOH, Roth, > 99%), styrene (S, Aldrich, distilled), THFMA (TCI, > 98%), vanillin (Thermo Scientific, 99%), 2,2'-azobis(isobutyronirtrile) (AIBN, Riedel-deHäen, > 98%), triethylamine (Merck, 99%) tetrahydrofuran (THF, Grüssing, 99%), tert-dodecanthiol (Merck, 98%), methanol (Walter CMP, 98.5%), hydroquinone (Fluka, 98%), toluene (Sigma Aldrich, 99.9%) were purchased.

Preparation of Vanillin Methacrylate: In a 1 L flask, 105 g (0.69 mol) vanillin was dissolved in 300 mL THF, followed by addition of 105.8 mL (0.75 mol) triethylamine. Once the vanillin was completely dissolved, 113.1 mL (0.75 mol) of methacrylic anhydride was added. The solution was stirred at 40 °C for 24 h. The organic phase was extracted twice with a saturated sodium chloride solution, twice with a saturated sodium bicarbonate solution, twice with 0.5 M sodium hydroxide solution, and twice with a saturated sodium chloride solution, followed by drying. The synthesis was adopted from reference Parkatzidis et al.[32]

Preparation of Copolymers: An amount of 40 mg of AIBN (0.24 mmol) was dissolved in 5 mL of toluene. Then, the monomers were added: 0.175 mL styrene (1.53 mmol, 1.05 mL HEMA (8.63 mmol), and monomer 3. As monomer 3 1.275 mL MMA (11.97 mmol), 1275 mL THFMA (7.79 mmol), or 2.3968 g VMA (10.8 mmol) was used. To limit the molar mass of the copolymers tert-dodecyl mercaptan (CTA) were added: 3 wt% (0.0744 g) for THFMA and VMA and 6 wt% (0.1488 g) for MMA. The composition of all reaction mixtures is given in Table S1 (Supporting Information). After purging the reaction solution with nitrogen for 15 min, the polymerization was performed in 10 mL vials inserted in a heating block at 60 °C, which was shaken with 100 rpm. The polymerization was stopped and the polymer precipitated by adding an ice-cold methanol/hydroquinone solution. Then, the product was filtered, washed with methanol, and dried. Three polymerizations were carried out. The composition of all reaction mixtures is given in Table S1 (Supporting Information). Since the copolymer was not fully soluble in the available eluents THF and *N*,*N*-dimethylacetamide for size-exclusion chromatography, information on the molar mass distributions is not available.

Cross-Linking of Copolymers: For cross-linking 0.1 g of the dry copolymer was dissolved in 1 mL of 1,4-dioxane and 0.8 mL of an MDI solution was added. For the MDI solution, 30.8 g of Desmodur VP.PU 10WB94 was dissolved in 100 mL of 1,4-dioxane. The reaction mixture contained in 20 mL vials was shaken at 100 rpm for 3 days. The resulting organogel was poured in a polypropylene container of 28 mm diameter and closed to avoid evaporation of the solvent. The organogels had a diameter of 28 mm and a height of 2 mm.

For cross-linking the copolymer with oligomeric MDI, the OH-number of the copolymer was determined assuming complete incorporation of HEMA into the copolymer. The MDI was specified with an NCO content of approx. 32% by the supplier. The given amount of MDI allowed for achieving a cross-linking level of 80 mol%.

Solvent Exchange and Supercritical CO_2 Drying: The solvent of the organogels 1,4-dioxane was exchanged with pure ethanol (EtOH, 99.8%, Carl Roth GmbH & Co. KG) until a minimum final concentration of 97.0 wt% EtOH inside the alcogel substrates was reached (controlled by density measurements, Anton Paar, DMA 4500 M). Subsequently, the alcogels were transferred into an autoclave and dried for 4 h using supercritical CO_2 at a flow rate of ≈120 g min^{-1} for 4 h at 125 bar and 70 °C. After slow

depressurization (≈2 bar min^{-1}), the dry samples were removed from the autoclave and stored in sealed vessels in a desiccator till further analysis.

Envelope and Skeletal Density: The envelope density of aerogels (ρ_e) was determined based on the mass and volume of the substrates:

$$\rho_e = \frac{m}{v} \tag{1}$$

with m being the mass determined by weighing the samples using a fine scale and v is the volume of the substrates determined using a vernier scale. The skeletal density (ρ_s) was determined via a helium pycnometer (Multivolume Micromeritics 1305, 6-fold measurement) at room temperature. The overall porosity ϵ was estimated via:

$$\varepsilon = \left(1 - \frac{\rho_e}{\rho_S}\right) \cdot 100 \tag{2}$$

Nitrogen Physisorption: The specific surface area of the aerogels was evaluated by nitrogen multilayer adsorption measured as a function of the relative pressure using a nitrogen adsorption Nova 3000e Surface Area Analyzer from Quantachrome Instruments and the (Brunauer–Emmett–Teller (BET) method. Estimation of the specific area via BET-method was based on BET-plots in the p/p_0 range of 0.03–0.27 (Figure S8, Supporting Information). A good applicability of the BET-method was indicated by high correlation of the BET-plots ($R^2 \geq 0.9997$) and BET C-constants in the range of 61–100.

The BJH method was used to determine the meso pore volume (V_{meso}), the pore size distribution, and the mean pore diameter (d_{mean}). All measurements were carried out as single determinations under an estimation of a relative measurement error of 5%.

Scanning Electron Microscopy (SEM): For characterization of the aerogel's inner pore structure via SEM (Zeiss Supra VP55, Jena, Germany) substrates were cut open with a razor blade and sputtered with a conductive, thin (approx. 6 nm) layer of gold (Sputter Coater SCD 050, BAL-TEC) before analysis. Measurements were performed under a high vacuum at an accelerating voltage of 3 kV. An in-lens detector at a working distance of 3.8 mm was used.

Contact Angle Measurements: Static water contact angles (STA) were determined utilizing a drop shape analyzer (OCA 15EC) using 1 µL of water in each run. The initial STA was measured immediately after deposition of the droplet on the substrates surface. To identify if the droplet was absorbed in the porous matrix, the droplet was allowed to remain on the surface for 180 seconds, and according STAs were recorded after residence times (T_R) of 30 and 180 s. All reported values represent an average of contact angles taken on both sides of the droplet on three individual substrates respectively.

IR Spectroscopy: IR spectra were measured with a BRUKER Alpha-T IR (4000 cm^{-1} to 400 cm^{-1}) in ATR mode.

Thermogravimetric Analysis: A TGA 2 instrument from Mettler Toledo was used for the analyses. Nitrogen atmosphere was applied for the analysis in a temperature range from 25 °C to 800 °C. Around 100 mg of substance was analyzed in a 900 µL Al_2O_3 crucible.

Uniaxial Compression Tests: In order to assess the mechanical strength of aerogel samples, uniaxial compression tests were performed using a Texture Analyser (TA.XTplusC, Stable Micro Systems). Hereby, the samples were compressed by a cylindrical piston (4 mm diameter), the compression force acting on the samples was varied in the range from 0 to 500 N. All tests were performed at a test speed of 0.15 mm s^{-1} and conducted at three different locations on each sample. The resulting force–distance curves were averaged and analyzed.

Laser Scanning Confocal Microscopy: The surface roughness of aerogel samples was tested using a Keyence 3D Laser Scanning Confocal Microscope VK-X160K. Images were captured at magnifications of 10× and 20× and the surface roughness was determined for two different areas of a sample over a line of 100 mm by multiple line analysis. Images were treated and analyzed using the "MultiFileAnalyzer VK-H1XMD" software by smoothing and filtering large deviation by Gaussian filter. The surface roughness was assessed using the profile roughness parameters (R_a, R_z, and R_{Sm}), as defined by the DIN EN ISO 4287 standards (Equations 3 – 5):

$$R_a = \frac{1}{l}\int_0^l |Z(x)|\,dx \tag{3}$$

with R_a being the arithmetic average of the absolute values of the roughness profile ordinates, Z the profile ordinates of the roughness profile, and l the sampling length.

$$R_z = \frac{1}{n}\left(R_{z1} + R_{z2} + \cdots + R_{zn}\right) \tag{4}$$

with R_z being the arithmetic mean value of the single roughness depths R_{zi} of consecutive sampling lengths.

$$R_{Sm} = \frac{1}{n}\sum_{i=1}^{n} S_{mi} \tag{5}$$

with R_{Sm} being the arithmetic mean value of the widths of profile elements of the roughness profile and S_m being the width between the peaks and valleys forming a profile element.

Supporting Information

Supporting Information is available from the Wiley Online Library or from the author.

Acknowledgements

C.A. and R.A. contributed equally to this work.
Open access funding enabled and organized by Projekt DEAL.

Conflict of Interest

The authors declare no conflict of interest.

Data Availability Statement

The data that support the findings of this study are available from the corresponding author upon reasonable request.

Keywords

bio-based monomers, radical polymerization, supercritical drying, water-repellent aerogels

Received: March 14, 2024
Revised: May 24, 2024
Published online: June 24, 2024

[1] S. Zhao, W. J. Malfait, N. Guerrero-Alburquerque, M. M. Koebel, G. Nyström, *Angew. Chem., Int. Ed.* **2018**, *57*, 7580.
[2] S. S. Kistler, *Nature* **1931**, *127*, 741.
[3] S. Basak, R. S. Singhal, *Food Hydrocolloids* **2023**, *141*, 108738.
[4] L. Baldino, S. Zuppolini, S. Cardea, L. Diodato, A. Borriello, E. Reverchon, L. Nicolais, *J. Supercrit. Fluids* **2020**, *156*, 104681.

[5] M. Lazrag, C. Lemaitre, C. Castel, A. Hannachi, D. Barth, *J. Supercrit. Fluids* **2018**, *140*, 394.
[6] A. Gandini, T. M. Lacerda, A. J. F. Carvalho, E. Trovatti, *Chem. Rev.* **2016**, *116*, 1637.
[7] A. Verma, S. Thakur, G. Goel, J. Raj, V. K. Gupta, D. Roberts, V. K. Thakur, *Curr. Res. Green Sustainable Chem.* **2020**, *3*, 100027.
[8] E. B. Yahya, F. Jummaat, A. A. Amirul, A. S. Adnan, N. G. Olaiya, C. K. Abdullah, S. Rizal, M. K. Mohamad Haafiz, H. P. S. A. Khalil, *Antibiotics* **2020**, *9*, 648.
[9] B. Schroeter, I. Jung, K. Bauer, P. Gurikov, I. Smirnova, *Polymers* **2021**, *13*, 3000.
[10] G. Wei, J. Zhang, M. Usuelli, X. Zhang, B. Liu, R. Mezzenga, *Prog. Mater. Sci.* **2022**, *125*, 100915.
[11] S. Takeshita, A. Konishi, Y. Takebayashi, S. Yoda, K. Otake, *Biomacromolecules* **2017**, *18*, 2172.
[12] H. Sai, R. Fu, L. Xing, J. Xiang, Z. Li, F. Li, T. Zhang, *ACS Appl. Mater. Interfaces* **2015**, *7*, 7373.
[13] H. Qin, Y. Zhang, J. Jiang, L. Wang, M. Song, R. Bi, P. Zhu, F. Jiang, *Adv. Funct. Mater.* **2021**, *31*, 2106269.
[14] M. Alnaief, S. Antonyuk, C. M. Hentzschel, C. S. Leopold, S. Heinrich, I. Smirnova, *Microporous Mesoporous Mater.* **2012**, *160*, 167.
[15] S. Antonyuk, S. Heinrich, P. Gurikov, S. Raman, I. Smirnova, *Powder Technol.* **2015**, *285*, 34.
[16] M. Lebedevaite, V. Talacka, J. Ostrauskaite, *J. Appl. Polym. Sci.* **2021**, *138*, 50233.
[17] C. Zhang, S. A. Madbouly, M. R. Kessler, *Macromol. Chem. Phys.* **2015**, *216*, 1816.
[18] G. Hayes, M. Laurel, D. MacKinnon, T. Zhao, H. A. Houck, C. R. Becer, *Chem. Rev.* **2023**, *123*, 2609.
[19] H. Fouilloux, C. M. Thomas, *Macromol. Rapid Commun.* **2021**, *42*, 2000530.
[20] J. P. A. Heuts, L. M. Muratore, T. P. Davis, *Macromol. Chem. Phys.* **2000**, *201*, 2780.
[21] U. Meier-Westhues, K. Danielmeier, P. Kruppa, E. P. Squiller, *Polyurethanes: Coatings, Adhesives and Sealants*, Vincentz, Hannover **2019**.
[22] T. Budtova, D. A. Aguilera, S. Beluns, L. Berglund, C. Chartier, E. Espinosa, S. Gaidukovs, A. Klimek-Kopyra, A. Kmita, D. Lachowicz, F. Liebner, O. Platnieks, A. Rodríguez, L. K. Tinoco Navarro, F. Zou, S. J. Buwalda, *Polymers* **2020**, *12*, 2779.
[23] M. Thommes, K. Kaneko, A. V. Neimark, J. P. Olivier, F. Rodriguez-Reinoso, J. Rouquerol, K. S. W. Sing, *Pure Appl. Chem.* **2015**, *87*, 1051.
[24] S. Zhao, W. J. Malfait, N. Guerrero-Alburquerque, M. M. Koebel, G. Nyström, *Angew. Chem., Int. Ed.* **2018**, *57*, 7580.
[25] M. P. Patel, M. Braden, *Biomaterials* **1989**, *10*, 277.
[26] K. Rajendrakumar, R. Dhamodharan, *Eur. Polym. J.* **2009**, *45*, 2685.
[27] J. Stouten, M. K. N. De Roy, K. V. Bernaerts, *Mater. Today Sustainability* **2023**, *22*, 100396.
[28] M. A. Aegerter, N. Leventis, M. Koebel, (Ed: S. A. Steiner Iii), *Springer Handbook of Aerogels*, Springer International Publishing, Cham **2023**.
[29] A. Zaman, F. Huang, M. Jiang, W. Wei, Z. Zhou, *Energy Built Environ.* **2020**, *1*, 60.
[30] S. Krainer, U. Hirn, *Colloids Surf., A* **2021**, *619*, 126503.
[31] S. J. Hitchcock, N. T. Carroll, M. G. Nicholas, *J. Mater. Sci.* **1981**, *16*, 714.
[32] K. Parkatzidis, S. Boner, H. S. Wang, A. Anastasaki, *ACS Macro Lett.* **2022**, *11*, 841.

